Institute of Navigation GPS-95,
Palm Springs, California, September 1995.

Experimental Demonstration of GPS for Rendezvous Between Two Prototype Space Vehicles

Kurt R. Zimmerman Dr. Robert H. Cannon, Jr.
Stanford University
Stanford, California 94305
kzimm@sun-valley.stanford.edu, cannon@sun-valley.stanford.edu

Abstract

The objective of this research is to demonstrate that Differential Carrier Phase GPS techniques can be employed as the primary means of sensing both the relative position and the relative attitude of two space vehicles in order to perform complex maneuvers such as multi-vehicle rendezvous and station-keeping in Low Earth Orbit. An experimental hardware system, consisting of a prototype space robot, target vehicle, and GPS system, has been devised to closely emulate real spacecraft. Since the experiments take place indoors where GPS satellite signals cannot be received, several GPS pseudolite transmitters have been built and installed around the perimeter of the laboratory to provide the GPS signals. The indoor GPS environment created by the close-range pseudolite transmitters poses additional constraints on the algorithms used to extract relative position and relative attitude from the carrier phase measurements. Therefore, a secondary objective of this research is to develop GPS for indoor sensing, where it has the potential to be applied to indoor mobile robots and to automated manufacturing systems. This paper presents the theoretical formulation and results of a rendezvous experiment between a prototype space robot vehicle and a passive target vehicle. An mpeg movie of this experiment can be viewed at http://sun-valley.stanford.edu/movies/movies.html.

1 Introduction

This work is motivated by the need to increase the efficiency and safety of assembly, maintenance, inspection, and repair tasks in the high-risk environment of Low Earth Orbit. Examples of such tasks include satellite retrieval, Orbital Replacement Unit (ORU) change-outs on satellites and the proposed space station, and assembly of modules and truss structures for advanced space missions. Currently these tasks are performed by astronauts through hundreds of hours of Extra-Vehicular Activity (EVA). Highly autonomous robot systems – managed at the *task level* by a ground or space-based supervisor – can make these tasks more routine and lower risk.

Communication bandwidth limitations and data delay between the robot and the human supervisor force the need for a highly autonomous robot that can react to unpredictable situations. The degree of autonomy required for such a robotic system can only be achieved through reliable, high-bandwidth on-board sensors that enable dynamic control loops to be closed at the local level. Specifically, in order to perform a rendezvous task or multi-vehicle station-keeping, it is necessary to sense the relative position and orientation between both vehicles. This research project takes advantage of Differential Carrier Phase GPS technology to perform a precise intercept and capture of a free-floating target by an autonomous free-flying space robot. This paper presents:

- The fundamental research issues involved in developing an indoor testbed for GPS-based rendezvous.
- A description of the hardware system that has been developed.
- The theoretical analysis for using GPS to sense two non-stationary vehicles.
- Practical implementation issues, results and conclusions from this experiment.

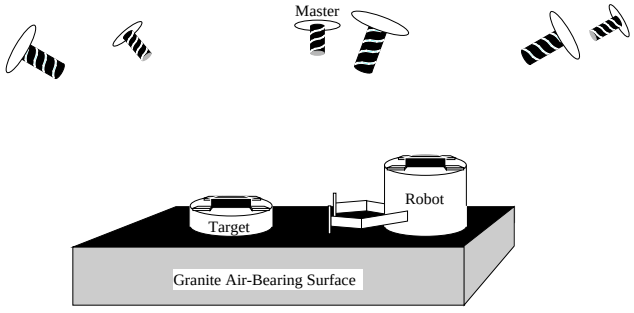

Figure 1: **Rendezvous Experiment Configuration**

2 Research Issues

There are several fundamental research issues that had to be addressed prior to the successful completion of this project, and prior to the use of GPS technology in a true space rendezvous mission. The issues addressed by this research are listed below. Related research issues have been studied by [1], [2] and [3]

The use of GPS as a sensor in real-time feedback control – GPS sensing is susceptible to both predictable and unpredictable loss of sensor data due to occlusion, vehicle configuration, and multipath. Partial loss of signal information can be compensated for with measurements from several satellites together with proper prediction using vehicle dynamics.

The use of GPS for indoor sensing – The prospect of using GPS indoors presents several fundamental problems, such as those initially discussed in [4]:

- *Spherical wavefronts* – Since the transmitters are very close to the workspace, the wavefront will be spherical rather than planar. This leads to nonlinear phase measurement equations from which the position and attitudes must be derived.

- *Lack of pseudorange* – Pseudorange (time-of-flight measurements) cannot be used indoors due to the relatively low accuracies available. The pseudolites are therefore not even designed to broadcast the data needed to calculate pseudorange. This resulted in the need to reformulate attitude and integer-resolution algorithms to meet this constraint [5].

- *High multipath environment* – Signal reflections off of walls can result in a much greater occurrence of multipath indoors than outdoors. This problem is being alleviated through the use of custom-designed helical antennas with conical-shaped beam patterns.

- *Near-far problem* – The close proximity of the transmitting sources to the receivers leads to very large variations in the power of the signal received as the vehicle traverses the workspace. The signal power of each of the pseudolites must be carefully adjusted so that the receiver does not cross-correlate signals (jam) at one extreme of the workspace and yet is still able to receive the signal at the other extreme of the workspace.

- *Calibration of a pseudolite positions and antenna baselines* – The locations of the phase centers of the pseudolite transmitter antennas and the vehicle receiver antennas need to be precisely determined before the necessary tolerances to perform rendezvous can be met.

Coordinated control of a multi-arm space robot – The Stanford Aerospace Robotics Lab (ARL) has already demonstrated the coordinated control of a multi-arm free-flying space robot for target rendezvous and capture [6]. These pioneering experiments were successfully demonstrated through the use of an overhead vision sensing system which was employed to provide the relative vehicle/satellite position and orientation. A constraint of this vision system is that it operates in only two dimensions and requires an overhead, perpendicular view of illuminated target points on each object in the workspace. The GPS system replaces the overhead vision system as the source of relative position and attitude information. Data from the vision system is still used as a means for evaluating the performance of the GPS system.

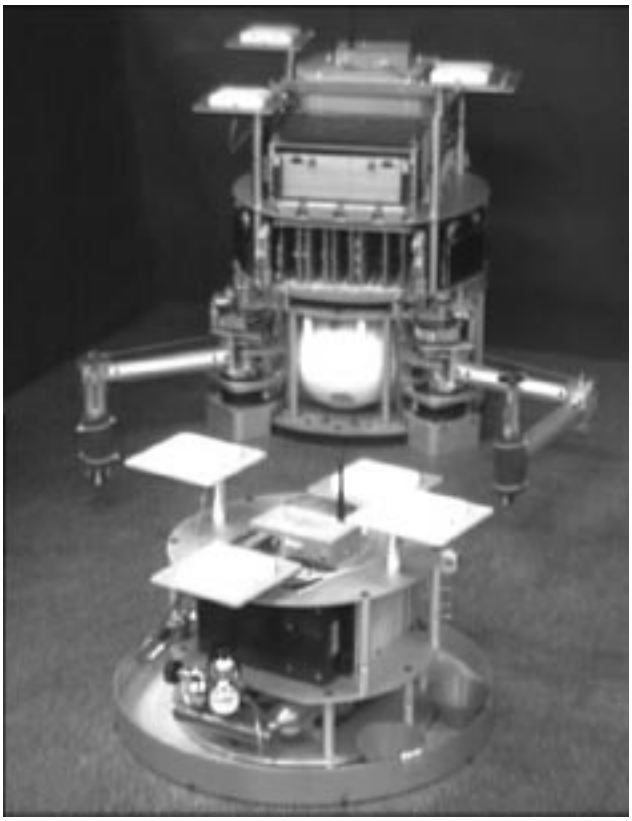

Figure 2: **ARL Free-Flying Space Robot and Target Vehicle**

3 System Description

Experiment Configuration – The experiment configuration is shown in Figure 1. GPS signals are generated by six pseudolites distributed around the laboratory above the workspace of the vehicle. The robot is commanded at an intuitive, task level through a graphical user interface to rendezvous and capture the moving target. The robot combines its phase measurements with the target's phase measurements to estimate the relative position and attitude and plan an intercept trajectory in real time. Once it is within capture range, the robot can grasp the target using its manipulators.

Robot and Target Vehicles – The robot and target vehicles are each equipped with a six-channel GPS receiver that is capable of multiplexing between four antennas, i.e. up to 24 carrier phase measurements on each vehicle, prior to taking differences. The receivers are off-the-shelf TANS Quadrex receivers from Trimble Navigation, with customized internal software. Carrier phase measurements from the target vehicle's GPS receiver are time-tagged and broadcast out through a 19.2k baud modem. The robot receives the measurements and combines them with its own measurements and processes them to derive position and orientation relative to the target vehicle. Specifically, the target broadcasts 18 differential carrier phase measurements and 6 raw carrier phase measurements at 10Hz (see Figure 6).

The robot, depicted in Figure 2. uses an air-cushion support system to achieve the drag-free, zero-g characteristics of space in two dimensions. It is a self-contained autonomous vehicle, complete with on-board VME-bus computers, radio-link Ethernet transceiver, batteries, cold-gas propulsion system with eight on-off thrusters, and dual cooperating manipulators. The control software is written in "C" and "C++" and is being developed using $ControlShell^{TM}$ [7] and the $VxWorks^{TM}$ Operating System.

The target vehicle, also depicted in Figure 2 is equipped with its own power, communication, and flotation devices.

Pseudolite Constellation – Each pseudolite produces its own L1 (1.575GHz) carrier phase signal modulated by its own unique C/A code. In order to perform differential carrier phase measurements between the robot and the target vehicle, the receivers on both vehicles must be synchronized to within one millisecond, so that the carrier phase measurements from each are tagged to the same millisecond epoch. Synchronization is achieved through a "Master Pseudolite" which broadcasts a 50bps GPS data signal modulated on top of the C/A code. This 50bps data signal contains valid timing information from which the two receivers can automatically synchronize, enabling differential carrier phase measurements between the two receivers. Figure 3 shows a mounted pseudolite (broadcasting as PRN 11). The pseudolite is completely self-contained, and can be mounted anywhere around the room on a standard track-lighting fixture

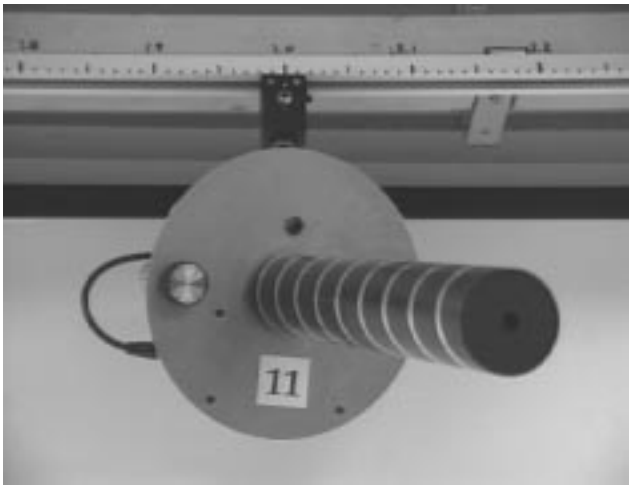

Figure 3: **Mounted Pseudolite**

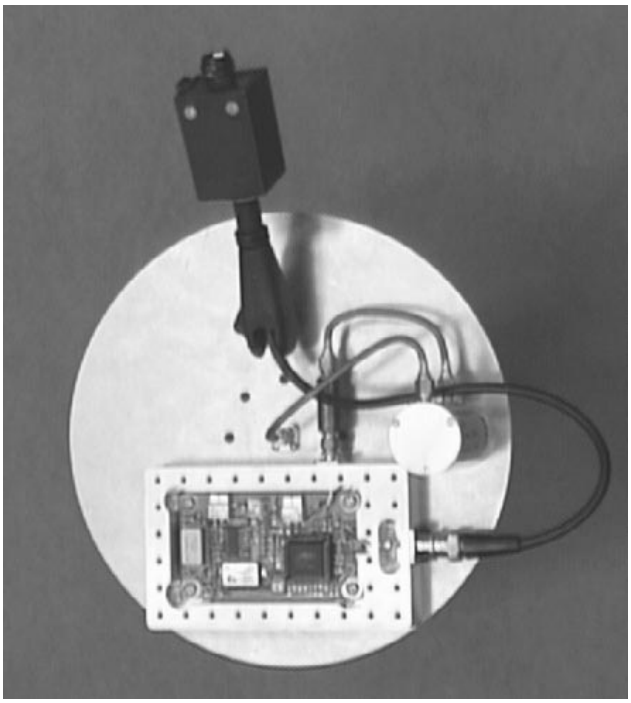

Figure 4: **Pseudolite Transmitter**

which supplies power at 12V. Figure 4 shows the internals of a GPS pseudolite transmitter box as it is mounted on the back of the helical antenna. For size reference, the ground plate of the antenna is 8.5" in diameter. The transmitter electronics board was designed by the Stanford GPS Laboratory for use on their automated landing system for aircraft [8]. The antenna is designed to broadcast L1 in the normal mode with a conical beam pattern.

Overhead Global Vision System – An overhead vision system (not shown) that is capable of tracking the robot and target vehicles also exists for evaluation of the GPS system performance. The vision system can track the vehicles at 60Hz, with an absolute accuracy estimated at better than than 2cm over the entire workspace and static noise of less than 1mm.

4 Theoretical Analysis

The rendezvous and station-keeping experiments require the estimation of the attitudes and positions of both vehicles. This section provides the derivation of the equations needed to compute the states of the vehicles from the GPS carrier phase measurements. Figure 5 shows the method in which the phase differences are taken and Figure 6 shows the variable definitions. The following assumptions and conventions are made in the derivation:

Assumptions

- The initial position of each vehicle is known. This means that as long as the pseudolites stay in lock after initialization, the integer ambiguity problem can be ignored [1].
- Pseudorange cannot be used in the formulation. The pseudolites do not provide the information required to perform pseudorange measurements since the accuracy of these measurements would be useless at very close range.
- The receivers provide measurements synchronized to within one millisecond. These measurements are further refined to effectively achieve much better than millisecond synchronization, as described in **Time Bias Corrections** below.
- The positions of the pseudolite transmitters are known and fixed.

[1] In the actual implementation, knowledge of the state and dynamics of the vehicles is used to recompute the integer values when pseudolite signals are lost or gained

Conventions

- Subscript i is always a *vehicle* index, j is an *antenna* index, and k is a *pseudolite* index; Subscript $j = m$ refers to the *master antenna* of a vehicle and $k = M$ refers to the *master pseudolite*.
- A plain-text Δ refers to the first-difference between antennas on the *same* vehicle; a **boldface** $\mathbf{\Delta}$ refers to the first-difference *between the master antennas of the two vehicles.*
- The attitude is alternatively represented as a rotation matrix, R_i, and also as an equivalent angle-axis vector, V_i. These representations are related to the quaternion state as shown below:

$$R_i = \begin{bmatrix} 1-2\epsilon_2\epsilon_2-2\epsilon_3\epsilon_3 & 2(\epsilon_1\epsilon_2-\epsilon_3\epsilon_4) & 2(\epsilon_1\epsilon_3+\epsilon_2\epsilon_4) \\ 2(\epsilon_1\epsilon_2+\epsilon_3\epsilon_4) & 1-2\epsilon_1\epsilon_1-2\epsilon_3\epsilon_3 & 2(\epsilon_2\epsilon_3-\epsilon_1\epsilon_4) \\ 2(\epsilon_1\epsilon_3-\epsilon_2\epsilon_4) & 2(\epsilon_2\epsilon_3+\epsilon_1\epsilon_4) & 1-2\epsilon_1\epsilon_1-2\epsilon_2\epsilon_2 \end{bmatrix}$$

$$V_i = \begin{bmatrix} \frac{2\epsilon_{i1}\cos^{-1}(\epsilon_{i4})}{\sin(\cos^{-1}(\epsilon_{i4})/2)} \\ \frac{2\epsilon_{i2}\cos^{-1}(\epsilon_{i4})}{\sin(\cos^{-1}(\epsilon_{i4})/2)} \\ \frac{2\epsilon_{i3}\cos^{-1}(\epsilon_{i4})}{\sin(\cos^{-1}(\epsilon_{i4})/2)} \end{bmatrix}$$

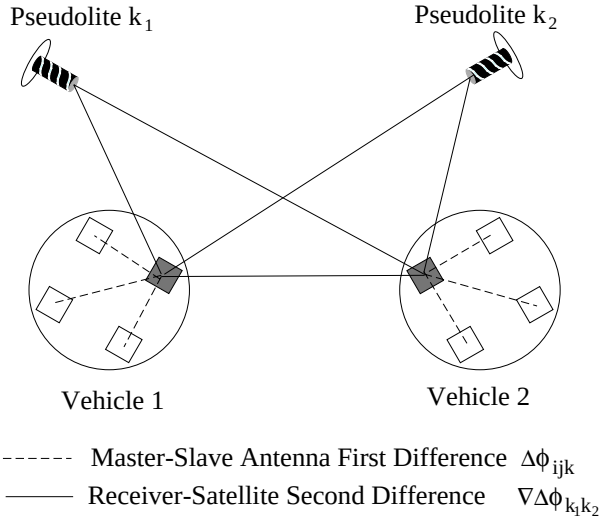

Figure 5: **Phase Difference Method**

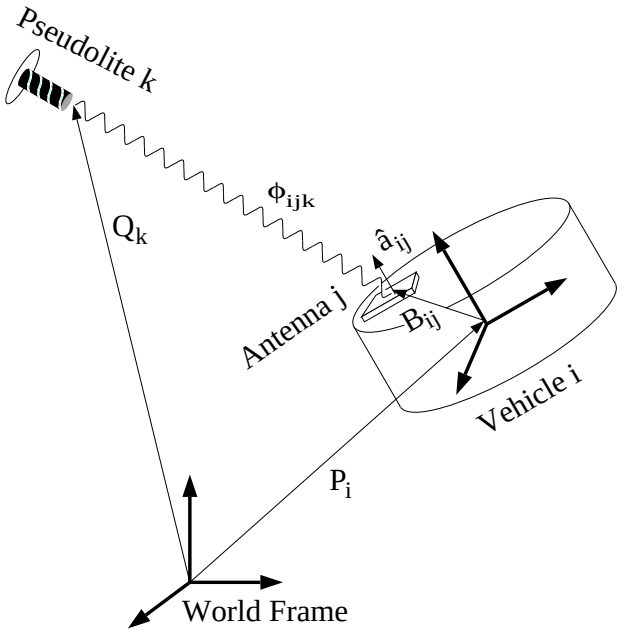

Figure 6: **Variable Definitions**

P_i	Position of vehicle i, in world frame
R_i	Attitude of vehicle i, in world frame (as rotation matrix)
B_{ij}	Baseline from vehicle center to antenna position, in vehicle frame
c	Speed of light
τ_{vi}	Receiver clock drift for vehicle i
τ_{pk}	Transmitter clock drift for pseudolite k
λ	GPS L1 carrier wavelength
K_{ijk}	Integer ambiguity between antenna j of vehicle i and pseudolite k
V_i	Attitude of vehicle i, in world frame (as equivalent angle-axis vector)
$\hat{a}_{ij}$	Antenna bore site vector of antenna j of vehicle i, in vehicle frame

The Unknown State

The state of each vehicle is represented as a 7x1 vector:

$$X_i = \begin{bmatrix} P_i \\ E_i \end{bmatrix} = \begin{bmatrix} p_{ix} \\ p_{iy} \\ p_{iz} \\ \epsilon_{i1} \\ \epsilon_{i2} \\ \epsilon_{i3} \\ \epsilon_{i4} \end{bmatrix} \quad (1)$$

where $\epsilon_{i1}, \epsilon_{i2}, \epsilon_{i3}$, and ϵ_{i4} are the four quaternion parameters that describe the attitude of the vehicle. The fourth quaternion ϵ_{i4} is constrained by the equation:

$$\epsilon_{i1}^2 + \epsilon_{i2}^2 + \epsilon_{i3}^2 + \epsilon_{i4}^2 = 1 \quad (2)$$

Measurement Equations

The measured carrier phase for vehicle i, antenna j, from pseudolite k is:

$$\begin{aligned} \phi_{ijk} &= |(P_i + R_i B_{ij}) - Q_k| + c\tau_{vi} + c\tau_{pk} + \\ &\quad \lambda K_{ijk} - V_i \cdot \hat{a}_{ij} \end{aligned} \quad (3)$$

The term $V_i \cdot \hat{a}_{ij}$ represents the change in the phase measurement due to antenna rotation in the circularly polarized field. If all the antenna bore sites are aligned on the vehicle, this term cancels after taking phase differences.

Master-Slave Antenna First Differences (for each vehicle):

The master-slave antenna first differences are used to determine the attitude of each vehicle. These are derived by taking the differences between the master antenna ($j = m$) and each of the slave antennas j of vehicle i for measurement from pseudolite k:

$$\begin{aligned} \Delta\phi_{ijk} &= |(P_i + R_i B_{im}) - Q_k| - \\ &\quad |(P_i + R_i B_{ij}) - Q_k| + \\ &\quad \lambda M_{ijk} - V_i \cdot (\hat{a}_{im} - \hat{a}_{ij}) \end{aligned} \quad (4)$$

where $M_{ijk} = K_{imk} - K_{ijk}$.

Receiver-Satellite Second Differences (between vehicles):

The receiver-satellite second differences are used to determine the relative positions between each vehicle. Starting with first differences between master antennas of each vehicle ($i \in \{1, 2\}$):

$$\begin{aligned} \Delta\phi_k &= |(P_1 + R_1 B_{1m}) - Q_k| - \\ &\quad |(P_2 + R_2 B_{2m}) - Q_k| + \\ &\quad c(\tau_{v1} - \tau_{v2}) + \lambda(K_{1mk} - K_{2mk}) + \\ &\quad V_1 \cdot \hat{a}_{1m} - V_2 \cdot \hat{a}_{2m} \end{aligned} \quad (5)$$

Given N pseudolites, there are N unique second differences between pseudolite k_1 and k_2 ($k_1 \neq k_2$). These differences are taken to eliminate the remaining effects due to clock errors $c(\tau_{v1} - \tau_{v2})$

$$\begin{aligned}\nabla\mathbf{\Delta}\phi_{k_1k_2} &= |(P_1 + R_1B_{1m}) - Q_{k_1}| - \\ &\quad |(P_2 + R_2B_{2m}) - Q_{k_1}| - \\ &\quad |(P_1 + R_1B_{1m}) - Q_{k_2}| + \\ &\quad |(P_2 + R_2B_{2m}) - Q_{k_2}| + \\ &\quad \lambda N_{k_1k_2} \end{aligned} \quad (6)$$

where $N_{k_1k_2} = K_{1mk_1} - K_{2mk_1} - K_{1mk_2} + K_{2mk_2}$.

Combining the Measurements

All of the measurements are coupled to the states of both vehicles, so all of the measurements must be combined to resolve these states. From equations (4), (6), and constraints (2) the complete set of measurements can be related to the vehicle states:

$$\begin{bmatrix} \Delta\phi_{1jk} \\ 0 \\ \Delta\phi_{2jk} \\ 0 \\ \nabla\mathbf{\Delta}\phi_{k_1k_2} \end{bmatrix} = \begin{bmatrix} h_1(X_1) \\ 1 - (\epsilon_{11}^2 + \epsilon_{12}^2 + \epsilon_{13}^2 + \epsilon_{14}^2) \\ h_2(X_2) \\ 1 - (\epsilon_{21}^2 + \epsilon_{22}^2 + \epsilon_{23}^2 + \epsilon_{24}^2) \\ h_{12}(X_1, X_2) \end{bmatrix} \quad (7)$$

where h_1 is a set of nonlinear functions of X_1, h_2 is a set of nonlinear functions of X_2, and h_{12} is a set of nonlinear functions of both X_1 and X_2. The optimal estimate of X_1 and X_2 can be solved using a Newton-Raphson algorithm as described in [9].

Note that for the case in which all pseudolites are in view by all antennas of both vehicles, the dimension of h_1 and h_2 is 18x1, and the dimension of h_{12} is 6x1. Adding the two constraints, there are a total of 44 measurements. This is far more than necessary to resolve the 14 state variables. The fewest number of pseudolites that can be in view and yet still resolve the states is three, so long as all three are in common between both vehicles. Since time is synchronized by a single master pseudolite, a fourth pseudolite is not needed to solve for time.

Time Bias Corrections

The equations derived thus far assume that the phase measurements $\phi_{ijk}(t)$ are taken at the same instant for both vehicles. In reality, this is not true. Each of $\phi_{ijk}(t)$ can be thought of as a "snapshot" of the carrier wave at time t. Since the receivers are only synchronized to within a millisecond by the data message that is broadcast by the master pseudolite [10], the error can be as large as the maximum observed carrier phase rate (Doppler $\approx$ 1kHz) times the receiver time bias ($\approx$ 1msec) times the wavelength (0.19m), which can be several centimeters. It is therefore necessary to estimate the measurement at time t, given only measurements at times t_k. This is done with a simple first-order expansion:

$$\begin{aligned}\phi_{ijk}(t) &= \phi_{ijk}(t_k) + \int_{t_k}^{t} \dot{\phi}_{ijk}(t)dt \\ &\approx \phi_{ijk}(t_k) + \\ &\quad \frac{\phi_{ijk}(t_k) - \phi_{ijk}(t_{k-1})}{t_k - t_{k-1}}(t - t_k) \end{aligned} \quad (8)$$

If the master pseudolite clock is assumed to be "true time", then the C/A code phase of the master pseudolite $\psi_M(t_k)$ is directly proportional to the time bias error $(t - t_k)$ and this can be used to compute the phase correction factor: (note here that the M subscript indicates that this is the code phase for the master pseudolite, $k = M$, and that the corrections are only applied to the phases used in the difference equations between the vehicles, where $j = m$).

$$\begin{aligned}\phi_{imk} &\approx \phi_{ijk}(t_k) + \\ &\quad \frac{\phi_{imk}(t_k) - \phi_{imk}(t_{k-1})}{t_k - t_{k-1}} K_\psi \psi_M(t_k) \end{aligned} \quad (9)$$

If ψ is measured in chips, then $K_\psi = 1/1.023\text{x}10^6$ sec/chip. All of the phases used in (6) are adjusted for receiver time bias using (9).

5 Implementation Issues

Several issues needed to be resolved before practical experiment implementation was possible. These were dealt with as follows:

Mitigation of Multipath Errors – The effects of multipath measurement errors are reduced by comparing the actual phase measurements with predicted phase measurements. Knowledge of vehicle dynamics and the current state are used to predict the next set of phase measurements through a Kalman filter. The new phase measurements are then compared with the predicted phases, and the difference between the two is bounded to produce an estimated phase that is used in the next computation of the vehicle state. Figure 7 is a diagram of how this is done. The signal ϕ_{err} is bounded by passing it through a sigmoid function, with linear gain and an adjustable cutoff level. The phase that is used in the next state computation ϕ_{est} is then the sum of the bounded error and the predicted phase. Note that for small values of ϕ_{err}, the value of ϕ_{est} is ϕ_{meas}, while for large values of

ϕ_{err}, the value of ϕ_{est} is $\phi_{pred} + cutoff_level$. If the value of ϕ_{err} is greater than one full integer wavelength, then it is assumed that an integer slip has occured and ϕ_{meas} is adjusted accordingly. The cutoff level of the sigmoid function was experimentally set to be 2.5cm for these experiments. Setting the cutoff level too high will miss the multipath errors; setting it too low is essentially running the control system "open-loop". This technique is a simple work-around to implementing a full extended Kalman filter that would incorporate both the dynamics of the vehicle and the nonlinear transformation from carrier phase measurements to the vehicle states.

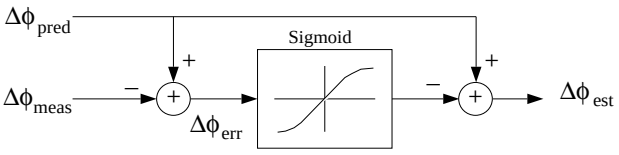

Figure 7: **Multipath Error Mitigation**

Near-far Problem and Occlusion – The near-far problem and occlusion of antennas by other antennas or vehicles results in a weak, unreliable measurement or complete loss of a signal. These problems are managed by having many more measurements available than necessary to solve the state estimate equations, and then reducing the set of valid signals for the solution. The method used to reduce multipath, as described above, can also reduce errors introduced by partially occluded signals. In order to deal with complete loss of signals, the algorithms that solve equation (7) were implemented to handle any combination of pseudolites in view by the two vehicles. The equations in (7) can be solved for any set of measurements, as long as at least three pseudolites are in common between both vehicles. For example, if vehicle 1 is locked on to five pseudolites, and vehicle 2 is locked on to four pseudolites, with three in common between them, then h_1 will be of dimension 15x1, h_2 will be of dimension 12x1, and h_{12} will be of dimension 3x1, and all available information is used in the solution.

Calibration of pseudolite positions and antenna baselines – A method to simultaneously calibrate the antenna baselines and pseudolite positions was implemented by considering equation (7) to be a function of unknown states B_{ij} and Q_k, with X_i known. The X_i were obtained from the global vision system, and data was collected for over one hundred vehicle locations over the workspace. This data was then used to obtain a least squares fit for the antenna baselines and pseudolite positions.

Integer ambiguity resolution – A motion-based algorithm has been developed and tested in simulation, but has not been implemented. The algorithm relies on spherical wavefront properties for resolving the integers and would be greatly enhanced in practice by incorporating other sensors, such as accelerometers, to increase the rate of convergence. For this experiment the integers were initialized by observing the vehicle locations with the overhead global vision system.

6 Results

Several experiments were carried out to demonstrate the functionality of the integrated GPS-controlled robot system. The most visual of these was the rendezvous experiment shown in the snapshot sequence on the following page. In this sequence, the target vehicle was given an initial velocity and the robot was commanded to follow a trajectory to close-in on the target. Once the target vehicle was within grasp range, the robot arms were commanded to track the gripper ports on the target. This was done using the relative position and orientation to infer the port locations on the target. Once the gripper ports were tracked, the robot lowered its grippers into the ports to grasp the target vehicle. Except for initialization, GPS was the only sensor used to complete this experiment. It has been shown that the robot can consistently grasp inside the the 9cm diameter gripper ports of the moving target vehicle.

Another experiment that was performed was autonomous station-keeping, in which the robot was commanded to hold station a fixed distance from the target and to follow the orientation of the target. The target vehicle was then manually perturbed in position and orientation and the robot followed. In order to get a sense for how well the robot can track the target, the vehicle's response to step inputs in position and orientation are shown in Figures 9 and 10. These plots also show a comparison between the GPS system and the global vision system. The static noise levels of the GPS system are summarized in the table of Figure 11. It is important to note that these are *static* noise levels, i.e. the RMS values of the noise observed when the vehicles remained in a fixed position and orientation. These do not reflect the effects of more serious error sources such as pseudolite and antenna baseline calibration errors, antenna phase-center stability, and multipath. These sources can create a "steady state" error of the vehicle position and attitude.

The comparison between the GPS and vision systems in the step response plots provide some sense of typical "steady state" errors in the GPS measurements (e.g. the orientation error appears to be approximately 3° around time $t = 15$ sec). The worst consequence of these errors is that when a pseudolite signal is acquired or lost, the recomputed integers for the new system configuration may be incorrect if the absolute position of either of the vehicles if off by more than half a wavelength (9.5cm), and the system needs to be re-initialized using the vision system.

7 Conclusions

The research presented in this paper has demonstrated a broad range of objectives:

- Established feasibility of performing rendezvous and station keeping using GPS as the primary means of sensing.
- Demonstrated an innovative use of GPS for indoor systems.
- Introduced a method for potentially testing GPS-based space systems end-to-end in lab prior to flight.
- Identified limitations and areas for improvement as GPS is developed for future space systems.

8 Acknowledgments

This research is supported under NASA Cooperative Contract NCC 2-333. The authors thank the members of the Stanford GPS Lab for their help and suggestions, and Trimble Navigation for not only supplying receiver hardware, but also offering the freedom to modify it for this research.

References

[1] Frank Bauer, E. Glenn Lightsey, et. al. Pre-Flight Testing of the SPARTAN GADACS Experiment. In *Proceedings of the Institute of Navigation GPS-94 Conference*, Salt Lake City UT, September 1994.

[2] A. Wayne Deaton Jorge I. Galdos, Triveni N. Upadhyay and James J. Lomas. GPS Relative Navigation for Automatic Spacecraft Rendezvous and Capture. In *Proceedings of the National Telesystems Conference*, Atlanta GA, June 1993.

[3] Lubomyr V. Zyla and Moises N. Montez. Use of two gps receivers in order to perform space vehicle rendezvous. In *Proceedings of the Institute of Navigation GPS-93 Conference*, Salt Lake City UT, September 1993.

[4] K. R. Zimmerman and R. H. Cannon Jr. GPS-Based Control for Space Vehicle Rendezvous. In *Proceedings of the ASCE: Robotics for Challenging Environments*, Albuquerque NM, February 28 - March 3 1994.

[5] Clark Emerson Cohen. *Attitude Determination Using GPS.* PhD thesis, Stanford University, Department of Aeronautics and Astronautics, Stanford, CA 94305, December 1992.

[6] M. A. Ullman. *Experiments in Autonomous Navigation and Control of Multi-Manipulator Free-Flying Space Robots.* PhD thesis, Stanford University, Stanford, CA 94305, March 1993. Also published as SUDAAR 630.

[7] S. A. Schneider, V. W. Chen, and G. Pardo-Castellote. ControlShell: A Real-Time Software Framework. In *Proceedings of the AIAA/NASA Conference on Intelligent Robots in Field, Factory, Service and Space*, volume II, pages 870–7, Houston, TX, March 1994. AIAA, AIAA.

[8] Clark E. Cohen, B. Pervan, et. al. Real-Time Flight Test Evaluation of the GPS Marker Beacon Concept for Category III Kinematic GPS Precision Landing. In *Proceedings of the Institute of Navigation GPS-93 Conference*, Salt Lake City UT, September 1993.

[9] Arthur E. Bryson, Jr. and Yu-Chi Ho. *Applied Optimal Control: Optimization, Estimation, and Control.* Hemisphere Publishing Corporation, 1025 Vermont Ave., N.W., Washington, D.C., 1975. Revised Printing.

[10] K. R. Zimmerman and R. H. Cannon Jr. GPS-Based Control for Space Vehicle Rendezvous. In *Proceedings of the Institute of Navigation GPS-94 Conference*, Salt Lake City UT, September 1994.

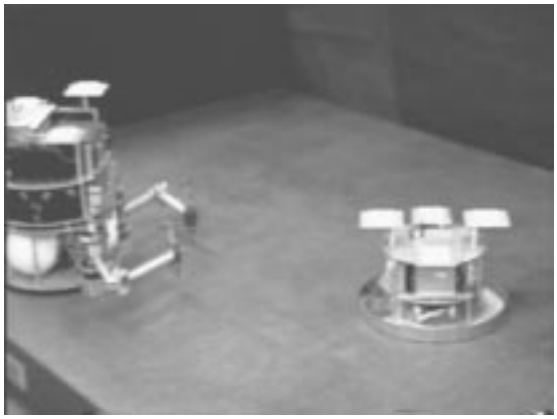

Figure 8: **Rendezvous Sequence**

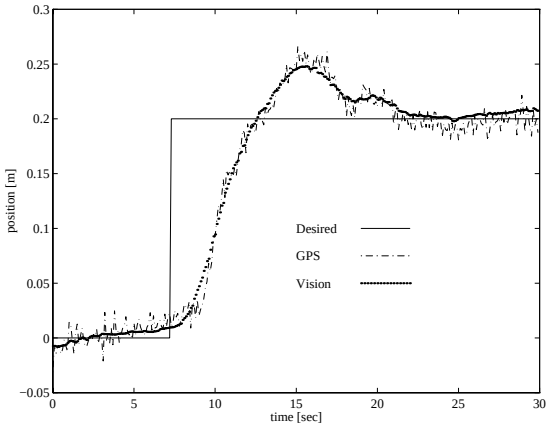

Figure 9: **Position Step Response**

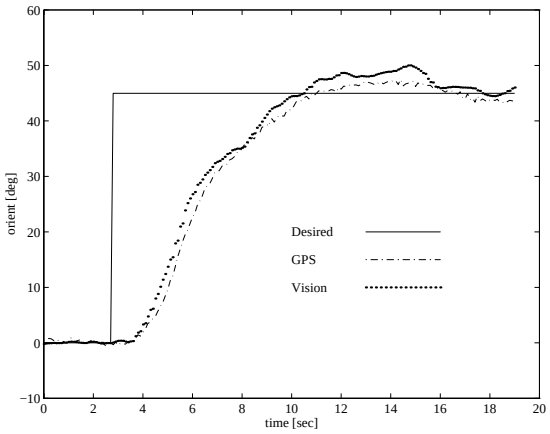

Figure 10: **Orientation Step Response**

Differential Position	0.5 cm
Absolute Position	6.0 cm
Differential Orientation	0.09°
Absolute Orientation	0.24°

Figure 11: **Static Noise Characteristics**